Semilocal properties of the Pauli kinetic potential

Lucian A. Constantin
Center for Biomolecular Nanotechnologies @UNILE, Istituto Italiano di Tecnologia, Via Barsanti, I-73010 Arnesano, Italy

(Received 8 February 2019; published 19 April 2019)

The logarithmic singularity of the Lindhard linear response function plays an important role in various phenomena, such as the long-range Friedel oscillations and Kohn anomaly in phonon dispersion. Such a weak singularity cannot be captured by the known gradient expansion of the kinetic energy (KE), but it can be somewhat mimicked by the second-order gradient singularity expansion (GSE2) developed in this work. We show that the GSE2 Pauli KE potential of atoms, computed with the Kohn-Sham density, is remarkably accurate, being the best possible approximation provided by any second-order KE gradient expansion. Next, we study the utility of GSE2 for orbital-free density functional theory, and we prove that the GSE2-based KE functionals give an important and systematic improvement over other popular KE functionals.

DOI: 10.1103/PhysRevB.99.155137

I. INTRODUCTION

The orbital-free density functional theory (OFDFT) [1,2] is a promising linear scaling $\mathcal{O}(N)$ method (here N is the number of electrons) [3,4] that finds the ground-state electron density $\rho(\mathbf{r})$, and implicitly all the ground-state properties, by solving the Euler equation [5]

$$\frac{\delta T_s[\rho]}{\delta\rho(\mathbf{r})}+v_{\rm ext}(\mathbf{r})+\int d\mathbf{r}'\frac{\rho(\mathbf{r}')}{|\mathbf{r}-\mathbf{r}'|}+\frac{\delta E_{xc}[\rho]}{\delta\rho(\mathbf{r})}=\mu, \quad (1)$$

where $v_{\rm ext}(\mathbf{r})$ is the external potential, μ is a Lagrange multiplier fixed from the normalization condition $\int d\mathbf{r}\ \rho(\mathbf{r})=N$, and $E_{xc}[\rho]$, $T_s[\rho]$ are the exchange-correlation (XC) and the noninteracting kinetic energy (KE) functionals, respectively. Both $E_{xc}[\rho]$, $T_s[\rho]$ must be approximated. The XC energy represents the many-body quantum effects beyond the Hartree approximation, being usually only a small fraction of the total energy and being accurately approximated by various XC functionals [6,7]. On the other hand, the KE of common matter (e.g., atoms and molecules) has the same order of magnitude as the total energy [8,9], therefore its approximation dictates the OFDFT accuracy.

Started with the seminal work of Thomas [10] and Fermi [11] (TF), over nine decades of intensive investigations did not succeed to provide an accurate and practical all-electron OFDFT, but important progress has been achieved [3,4,12–16], and various OFDFT large scale applications have been successfully performed [17–29]. The reason for this slowness is related to the highly nonlocal nature of the exact $T_s[\rho]$ [30–35], especially at the nuclear cusp [34,36–39], in the tail of the density [34,40–42], and at the inflection points of the density [38,42–44].

The KE functional is usually separated in two main contributions:

$$T_s[\rho]=T_s^W[\rho]+T_s^\theta[\rho], \quad (2)$$

with

$$T_s^W[\rho]=\int d\mathbf{r}\ \tau^W(\mathbf{r}),\quad \tau^W(\mathbf{r})=\frac{|\nabla\rho(\mathbf{r})|^2}{8\rho(\mathbf{r})}=\tau^{TF}(\mathbf{r})\frac{5}{3}s(\mathbf{r})^2 \quad (3)$$

being the von Weizsäcker KE functional [45], which is exact for any one- and two-electron spin-singlet state systems, as well as for the ground-state KE of any bosonic system. The $T_s^\theta[\rho]$ is called the Pauli KE functional, and it represents all many-body fermionic effects [46–54]. Note that while T_s^W has a simple semilocal exact expression, there are many approximations for the unknown $T_s^\theta[\rho]$ classified as: generalized gradient approximations (GGAs), e.g. [12,13,15,55–71], Laplacian-dependent meta-GGAs, e.g. [15,72–76], Hartree-potential dependent u-meta-GGAs, e.g. [77,78], and nonlocal approximations [14,79–90]. These functionals have been usually constructed from exact conditions and fitting to various data benchmarks, but we also acknowledge the emerging machine learning techniques [35,76,91–97] that may boost the OFDFT accuracy. Here $\tau^{TF}=(3/10)k_F^2\rho$ is the Thomas-Fermi (TF) KE density [10,11], with the Fermi wave vector being $k_F=(3\pi^2\rho)^{1/3}$, and $s=|\nabla\rho|/(2k_F\rho)$ is the reduced gradient of the density.

Up to date, the most sophisticated Pauli KE nonlocal functionals have been constructed from the linear response of the uniform electron gas (UEG), for which the central quantity is the Lindhard function [31]

$$F^{\rm Lind}=\left(\frac{1}{2}+\frac{1-\eta^2}{4\eta}\ln\left|\frac{1+\eta}{1-\eta}\right|\right)^{-1} \quad (4)$$

that is related to the density response $\chi^{\rm UEG}$ via:

$$-\frac{1}{\chi^{\rm UEG}}=\frac{\pi^2}{k_F}F^{\rm Lind}. \quad (5)$$

Here $\eta=k/(2k_F)$ is the dimensionless momentum. At $\eta=1$, there is a weak, logarithmic singularity in the slope of the Lindhard function, then

$$\lim_{\eta=1}\chi^{\rm UEG}=-\frac{k_F}{2\pi^2},\quad \lim_{\eta=1}\frac{\partial}{\partial\eta}\chi^{\rm UEG}=\infty. \quad (6)$$

This behavior is responsible for long-range Friedel oscillations [31,98]. For example, a point impurity in a three-dimensional (3D) UEG will produce an induced charge

density $\delta\rho$ which decays asymptotically as [1,31,99]

$$\lim_{r\to\infty} \delta\rho \propto \cos(2k_F r + \phi)/r^3, \tag{7}$$

with ϕ being a phase shift dependent on the impurity. Note that the singularity in the UEG dielectric response at $\eta = 1$ is present for all dimensions [99,100]. The KE gradient expansion of any finite order is reasonably accurate until $\eta < 1$ (see Fig. 7 of Ref. [31]) but cannot capture the logarithmic singularity at $\eta = 1$, such that the extensions of the Thomas-Fermi method, as semilocal OFDFT, cannot yield the Friedel oscillations and the atomic shell structure of the density, which are of the same origin [1,31,101,102]. Moreover, the logarithmic singularity occurs for various (anisotropic) Fermi surfaces of electron liquids [103], playing an important role in several physical phenomena, such as the Kohn anomaly in phonon dispersion [104].

The gapped UEG (gUEG) model [14,62,105–116], also called jellium-with-gap, is a generalization of the UEG that depends on the dimensionless ingredient $\Delta = E_g/E_F$, with E_g being the gap energy and $E_F = k_F^2/2$ the Fermi energy. Levine and Louie [105] derived a simple analytical form for the linear response function of the jellium-with-gap $F^{\rm GAP}$, which recently has been analyzed in detail and used to develop semilocal [62] and nonlocal [14] KE functionals. At $\eta = 1$, $\frac{\partial}{\partial\eta}\chi^{\rm gUEG}$ is dependent on Δ, being in general finite, with the exception of $\Delta \to 0$ limit, when it behaves as

$$\lim_{\eta=1} \frac{\partial}{\partial\eta}\chi^{\rm gUEG} \propto -\ln(\Delta). \tag{8}$$

Then, only for $\Delta = 0$, which represents the true UEG case, the logarithmic singularity is present.

In this work, we investigate the importance of the singularity at $\eta = 1$ in the linear response of GGA KE functionals, showing that it is closely related to the Pauli KE potential of atoms. The paper is organized as follows. In Sec. II, we present our theoretical results on the semilocal properties of the KE functional derivative. In Sec. III we incorporate these KE conditions into simple GGA functionals, and we perform a careful assessment of their OFDFT performance for atoms and ions. Finally, in Sec. IV we summarize our results.

II. THEORY

A. The KE second-order gradient singularity expansion

Let us consider a GGA kinetic functional of the form

$$T_s^{\rm GGA}[\rho] = \int d\mathbf{r}\ \tau^{TF}(\mathbf{r}) F_s^{\rm GGA}(s(\mathbf{r})), \tag{9}$$

where $F_s^{\rm GGA}$ is the KE enhancement factor, which we assume to have the correct formal expression in the slowly-varying density regime

$$F_s^{\rm GGA} \to 1 + \mu s^2, \quad \text{when} \quad s \to 0. \tag{10}$$

The linear response of such a functional

$$F(\eta) = \frac{k_F}{\pi^2}\mathcal{F}\left(\frac{\delta^2 T_s^{\rm GGA}[\rho]}{\delta\rho(\mathbf{r})\delta\rho(\mathbf{r}')}|_{\rho_0}\right), \tag{11}$$

where $\mathcal{F}$ represents the Fourier transform, can be straightforwardly computed using the following elegant approach

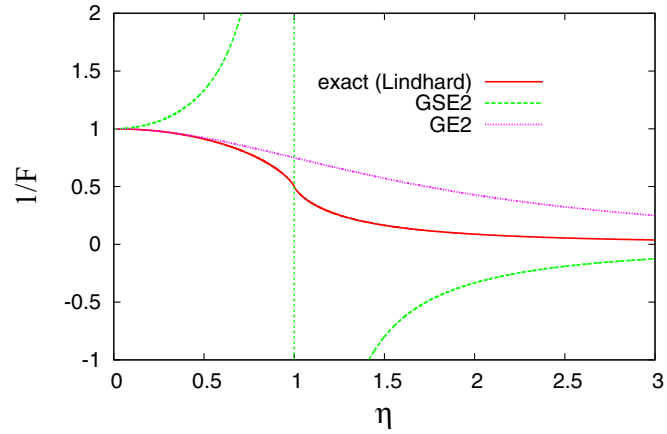

FIG. 1. The GSE2 [see Eq. (13)] and GE2 UEG linear responses, compared with the exact curve $1/F^{\rm Lind}$. Note that any GGA that recovers the GSE2 (GE2), at small variations of the density (when $s \to 0$), has the same UEG linear response as GSE2 (GE2), see Ref. [118].

[62,117]: Consider a small perturbation in the UEG density ρ_0 at $\mathbf{r} = \mathbf{0}$, such that the density is $\rho = \rho_0 + \rho_k e^{i\mathbf{kr}}$. Then, at $\mathbf{r} = \mathbf{0}$, we obtain $\rho = \rho_0 + \rho_k$, $\nabla\rho = \rho_k i\mathbf{k}$, and $\nabla^2\rho = -\rho_k k^2$. Using them in the GGA expression, the linear response is obtained as twice the second-order coefficient of the series expansion with respect to ρ_k/ρ_0. Then, the GGA linear response function is

$$F = 1 + \tfrac{9}{5}\mu\eta^2. \tag{12}$$

For details on derivation of Eq. (12), see Ref. [118]. The only way to obtain a singularity of $(\partial\chi/\partial\eta)|_{\eta=1}$ at the GGA level is to chose $\mu = -5/9$, which defines the following second-order gradient singularity expansion (GSE2) KE enhancement factor

$$F_s^{\rm GSE2} = 1 - \tfrac{5}{9}s^2 + \gamma q, \tag{13}$$

with γ being a positive constant and $q = \nabla^2\rho/[4(3\pi^2)^{2/3}\rho^{5/3}]$ the reduced Laplacian of the density. The UEG linear response of any GGA functional that recovers GSE2 in the slowly-varying density regime is reported in Fig. 1. Due to the strong and unphysical singularity at $\eta = 1$, this functional fails obviously in the k space, being exact only at $\eta = 0$, and in the asymptotic limit $\eta \to \infty$, such that it is not useful for solid-state OFDFT calculations. Also shown in Fig. 1 is the UEG linear response of any GGA functional that recovers the second-order gradient expansion (GE2).

The linear term γq in Eq. (13) does not contribute to the linear response, does not change the total KE because $\int d\mathbf{r}\ \tau^{TF} q = 0$ for any finite system and extended system under periodic boundary conditions [119], does not contribute to the functional derivative $\delta T_s[\rho]/\delta\rho$ (and implicit to the Pauli KE potential), but is very important for the quality of the KE density τ. The recent interest for accurate τ models [120–123] makes us also consider this linear term. Minimizing the quality factor [59,60,124]

$$\delta(\gamma) = \frac{1}{N}\int d\mathbf{r}\ |\tau^{\rm exact}(\mathbf{r}) - \tau^{\rm approx}(\mathbf{r},\gamma)|, \tag{14}$$

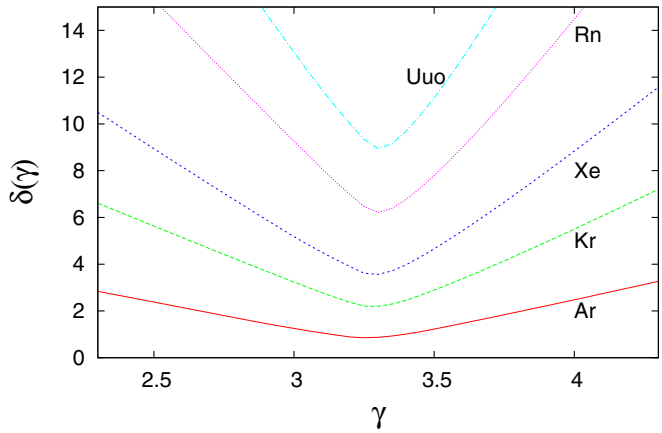

FIG. 2. The quality factor $\delta(\gamma)$ of Eq. (14), for noble atoms (from Ar to Uuo). We use KSDFT atomic orbitals and densities.

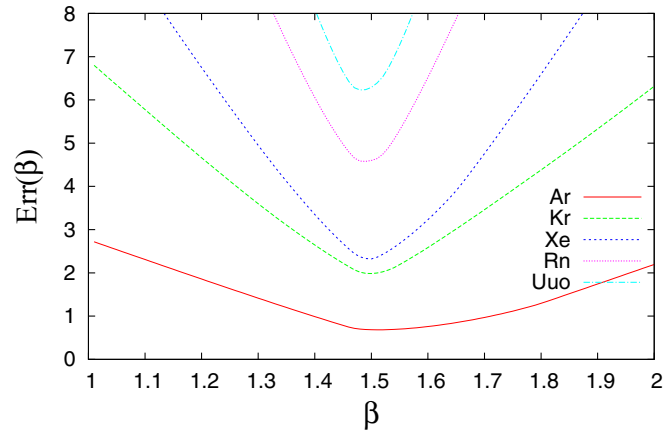

FIG. 3. The $\mathrm{Err}(\beta)$ function of Eq. (22), for noble atoms (from Ar to Uuo). We use KSDFT atomic orbitals and densities. Note that $\beta = 1$ and $3/2$, represent the GE2 and GSE2, respectively.

where $\tau^{\mathrm{exact}}(\mathbf{r})$ is the positive-defined Kohn-Sham (KS) DFT KE density, we find $\gamma = 3.3$. In Fig. 2, we show $\delta(\gamma)$ for noble atoms. For each atom, the minimum occurs at $\gamma \approx 3.3$, being bigger than the corresponding GE2 Laplacian coefficient. We recall that the GE2 enhancement factor is $F_s^{\mathrm{GE2}} = 1 + 5s^2/27 + 20q/9$, being very different from F_s^{GSE2} of Eq. (13).

The KSDFT and OFDFT calculations are all-electron calculations, performed with a modified version of the Engel code [125,126], which uses numerical orbitals and densities computed on a logarithmic grid on the radial direction. The Euler equation was implemented in the form of Eq. (1) of Ref. [5]. We use the LDA exchange functional with no correlation. This simple choice for the XC functional permits a better understanding of the KE functional performance in the OFDFT context.

To conclude this subsection, we recall several KE gradient expansions with negative coefficient of the gradient term

$$\begin{aligned} &\text{Airy gas,} \quad \text{Ref. [61];} \quad F_s(s,q) = 1 - 5s^2/27 + 10q/3, \\ &\text{empirical,} \quad \text{Ref. [75];} \quad F_s(s,q) = 1 - 0.275s^2 + 2.895q, \\ &\text{empirical,} \quad \text{Ref. [123];} \quad F_s(s,q) = 1.069 - 0.407s^2 + 5.84q, \end{aligned} \tag{15}$$

and all of them have strong singularities for UEG linear response but none at the right position $\eta = 1$.

B. Properties of Pauli potential for atoms

The Pauli potential for any finite system with spherical symmetry is [127,128]

$$v_\theta = \frac{\tau - \tau^W}{\rho} + \frac{1}{\rho}\sum_{i=1}^{N}(\epsilon_N - \epsilon_i)2\phi_i^2, \tag{16}$$

with ϕ_i being the ith occupied Kohn-Sham orbital.

For a single shell with density ρ_{nl}, where n, l are the principal and angular quantum numbers, the positive-defined KE density is [34]

$$\tau_{nl} = \tau_{nl}^W + \frac{l(l+1)}{2}\frac{\rho_{nl}}{r^2}. \tag{17}$$

Combining Eqs. (16) and (17), we obtain for regions dominated by a single shell

$$v_\theta = \frac{l(l+1)}{2}\frac{1}{r^2} + \frac{1}{n}\sum_{i=1}^{N}(\epsilon_N - \epsilon_i)2\phi_i^2. \tag{18}$$

A straightforward application of Eq. (18) is the asymptotic behavior in the tail of the density (when $r \to \infty$), where the Pauli potential behaves as

$$v_\theta \to \frac{l(l+1)}{2}\frac{1}{r^2}. \tag{19}$$

In order to understand if a gradient expansion can describe the Pauli potential in the atomic core, let us consider the following expression

$$v_\theta^{\mathrm{app}}(\beta) = \frac{\delta T_s^{TF}}{\delta\rho} - \beta\frac{8}{9}\frac{\delta T_s^W}{\delta\rho}, \tag{20}$$

where β is a parameter, and

$$\begin{aligned} \frac{\delta T_s^{TF}}{\delta\rho} &= \frac{d\tau^{TF}}{d\rho}, \\ \frac{\delta T_s^W}{\delta\rho} &= \frac{|\nabla\rho|^2}{8\rho^2} - \frac{\nabla^2\rho}{4\rho} \end{aligned} \tag{21}$$

are the functional derivatives of the Thomas-Fermi and von Weizsäcker functionals. Note that Eq. (20) spans all possible second-order gradient expansions (with $F_s = 1 + \mu s^2$, μ being a real number), by varying β.

When $\beta = 0$, 1, or 9/8 then $v_\theta^{\mathrm{app}}(\beta)$ corresponds to v_θ^{TFW}, v_θ^{GE2}, and v_θ^{TF}, respectively. To find β that gives the most accurate Pauli potential for atoms, we minimize the following error:

$$\mathrm{Err}(\beta) = \frac{1}{N}\int d\mathbf{r}\ \rho(\mathbf{r})\left|v_\theta^{\mathrm{exact}} - v_\theta^{\mathrm{app}}(\beta)\right|, \tag{22}$$

and the results are reported in Fig. 3 for noble atoms and in Fig. S1 of Ref. [118] for alkaline earth (from Mg to Ra) and closed-shell transition metal atoms (from Zn to Cn). The minimum is found for $\beta = 3/2$ that represents the GSE2 of Eq. (13). This result proves that GSE2 contains important

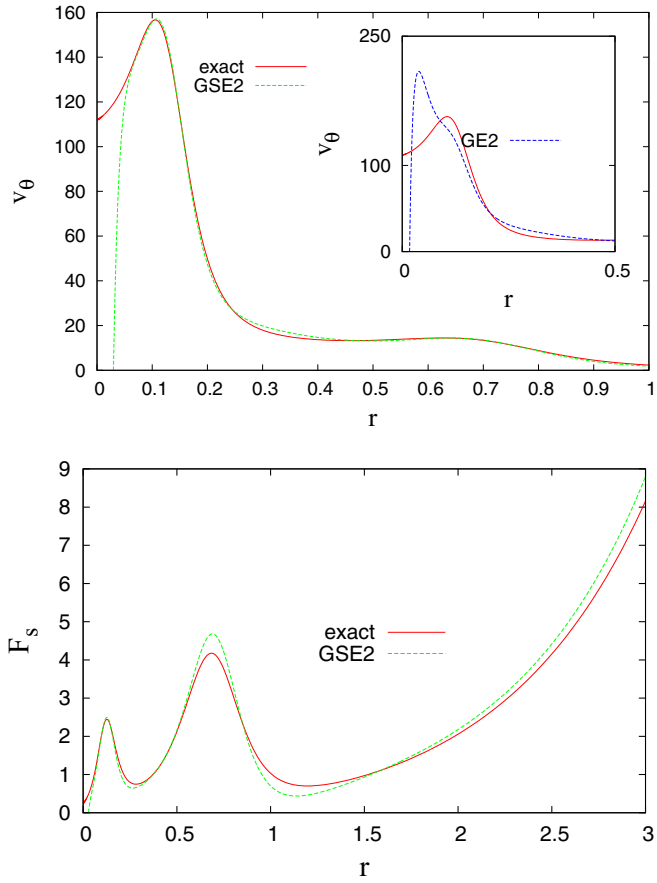

FIG. 4. Comparison between the exact and GSE2 Pauli kinetic potentials v_θ (upper panel), and KE enhancement factors F_s (lower panel), for the Ar atom. We use KSDFT orbitals and densities. The inset shows the GE2 Pauli kinetic potential of the Ar atom.

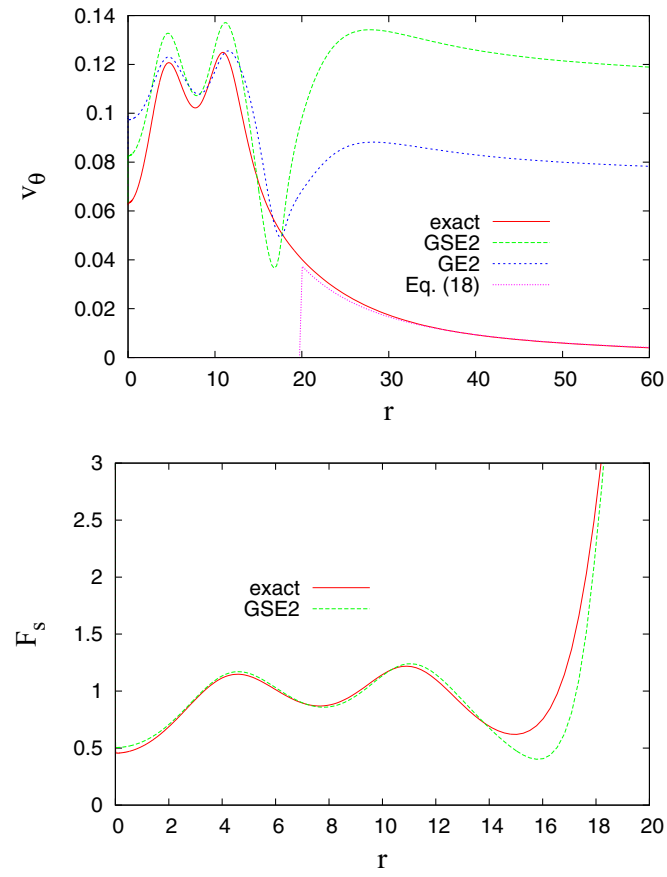

FIG. 5. Pauli kinetic potential v_θ (upper panel), and KE enhancement factor F_s (lower panel), versus the radial distance r, for the jellium cluster with 92 electrons and bulk parameter $r_s = 4$. We use KSDFT orbitals and densities.

physics that has not yet been investigated. We remark that Eq. (22) has similar scaling properties as Eq. (14) under the uniform scaling of the density $[\rho_\lambda(\mathbf{r}) = \lambda^3\rho(\lambda\mathbf{r})$, with $\lambda \geqslant 0]$, and, as shown below, can well capture the atomic shell structure of v_θ.

In Fig. 4, we report the GSE2 performance for Pauli kinetic potential and KE enhancement factor, in case of the Ar atom. Similar results, not shown here, are found for all noble atoms. Results for Mg and Zn atoms are reported in Fig. S2 of Ref. [118]. GSE2 can well reproduce the shell structure of both v_θ and F_s, when the KSDFT density is used. This is a significant achievement of the semilocal theory that should be further explored. Nevertheless, the region near the nucleus cannot be accurately described by the GSE2. Here the Laplacian diverges ($\nabla^2\rho \to -\infty$), the nonlocality becomes important [36,78], but still the von Weizsäcker KE functional is a good approximation [34].

Finally, in Fig. 5, we show the GSE2 performance for the jellium cluster with $N = 92$ electrons and bulk parameter $r_s = 4$, which has the radius $R_c = r_s N^{1/3} \approx 18.1$ a.u. Inside the jellium sphere, for $r \leqslant R_c$, the GSE2 is able to describe well both v_θ and F_s, capturing all the quantum shell oscillations. Outside the cluster, in the tail of the density, Eq. (19) becomes accurate, and the GSE2 fails to be a good approximation.

III. APPLICATIONS

A. GGA KE functionals that recover the GSE2

Let us consider the Pauli-Gaussian-μ (PGμ) family of GGA KE functionals, which have the Pauli KE enhancement factor [15]

$$F_s^\theta(s) = e^{-\mu s^2}. \tag{23}$$

For any $\mu \geqslant 0$, the exact important conditions are fulfilled by construction

$$F_s^\theta(s) \geqslant 0,$$
$$F_s^\theta(s = 0) = 1.$$

An attractive functional for OFDFT local-pseudo-potential-based solid-state calculations is PG1, being remarkably accurate for equilibrium volume, bulk modulus, total energy, and density error of metals and semiconductors, as shown in Fig. 1 and Table 1 of Ref. [15]. On the other hand, the PG$\frac{40}{27}$, called also PGS (from Pauli-Gaussian second order) because it recovers the GE2 in the slowly-varying density regime, is slightly better than PG1 for semiconductors but almost twice worse for metals. Moreover, when μ increases slowly, the accuracy of PGμ for metals is rapidly falling down.

The PG$\frac{20}{9}$ is the only functional from the PGμ family that recovers GSE2. This functional, that gives the UEG linear

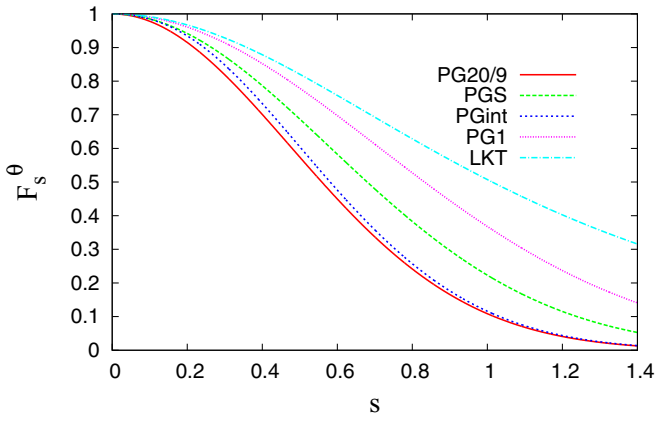

FIG. 6. Pauli KE enhancement factors F_s^θ of several GGA functionals. Note that $F_s^\theta = 1$ and 0 represent the TFW and W functionals, respectively.

response shown in Fig. 1, is not suited for OFDFT solid-state calculations. We also propose an interpolation between PG$\frac{20}{9}$ and PGS. We call this KE GGA functional PGint, because of similarities with PBEint exchange enhancement factor [129–131], having the following expression

$$F_s^{\theta,\mathrm{PGint}}(s) = e^{-\mu(s)s^2},$$
$$\mu(s) = \mu_1 + (\mu_2 - \mu_1)\frac{\alpha s^2}{1+\alpha s^2}, \qquad (24)$$

with $\mu_1 = 40/27$, $\mu_2 = 20/9$, and the parameter $\alpha = 10$ has been chosen such that PGint will be close to PG$\frac{20}{9}$ for $s \geqslant 0.2$. Nevertheless, because PGint recovers GE2 when $s \to 0$, its UEG linear response is represented by the GE2 one. In Fig. 6, we show a comparison between the PGint, PG20/9, PGS (a.i. PG40/27), and the Luo-Karasiev-Trickey (LKT) GGA [71] Pauli KE enhancement factors. We recall that LKT is very accurate for OFDFT local-pseudo-potential-based solid-state calculations [71]. By construction, PGint recovers PGS only at small gradients ($s \leqslant 0.2$), otherwise being close to PG$\frac{20}{9}$.

Finally, we mention that any GGA cannot recognize the nuclear region (where $s \approx 0.4$) from other atomic shells, and all the functionals of Fig. 6 are not accurate at the nuclear cusp. On the other hand, they are recovering the accurate von Weizsäcker at large gradients, behaving well in the asymptotic region, where the density decays exponentially.

B. Kinetic energy of noble atoms

We perform OFDFT calculations using several KE functionals (TFW, PG$\frac{20}{9}$, PGS, PG1, PGint, and LKT) for noble atoms, from He up to the atom with 290 electrons. We test only KE functionals that have positive Pauli enhancement factors ($F_s^\theta \geqslant 0$), such that from the λTFW family of functionals [15,70,132,133], we chose only the TFW functional. All calculations converged well, with an accuracy criterion less than 10^{-7} in the absolute value of the maximum deviation between the effective potentials (see Eq. (2) of Ref. [5]) of successive iterations. We recall that such atoms have been used to better understand the connection between DFT and semiclassical atom theory [134–138], to derive modified gradient expansions of the kinetic and exchange energies [75,78,139], to construct and investigate kinetic and exchange functionals [74,132,140–145], or to suggest that the periodic table of atoms with infinity number of electrons becomes perfectly periodic [146].

TABLE I. Exact KSDFT noninteracting KE, and relative errors in % ([approx-exact]/exact × 100), of noninteracting KE computed either self-consistently, within the OFDFT scheme (upper panel), or non-self-consistently, using accurate KSDFT densities (lower panel), from various KE functionals, for nonrelativistic noble atoms ($2 \leqslant Z \leqslant 290$). Last line of the panels reports the mean absolute relative error (MARE), in %. Best result of each line is shown in bold style.

Atom	KSDFT	TFW	PG$\frac{20}{9}$	PGS	PG1	PGint	LKT
Self-consistent calculations							
He	2.72	−41.6	**−12.0**	−18.9	−25.2	−12.8	−29.4
Ne	127.49	−31.1	5.0	−6.8	−15.1	**2.6**	−19.0
Ar	524.52	−27.5	6.7	−5.0	−13.0	**4.0**	−16.4
Kr	2746.87	−23.0	7.8	**−3.1**	−10.3	4.7	−13.1
Xe	7223.66	−20.6	7.8	**−2.4**	−9.1	4.6	−11.6
Rn	21852.32	−18.0	7.4	**−1.9**	−7.8	4.2	−10.0
Uuo	46303.50	−16.4	7.0	**−1.5**	−7.0	3.9	−9.0
168 e^-	106998.43	−14.8	6.5	**−1.3**	−6.3	3.5	−8.0
218 e^-	198231.01	−13.6	6.2	**−1.1**	−5.7	3.2	−7.4
290e^-	389334.88	−12.5	5.7	**−1.0**	−5.2	2.9	−6.7
MARE	–	21.9	7.2	**4.3**	10.5	4.6	13.1
Using KSDFT orbitals and densities							
He		88.5	**29.2**	40.1	50.9	30.9	58.6
Ne		61.5	**8.4**	19.5	29.9	10.5	36.4
Ar		51.3	**2.4**	13.5	23.4	4.8	29.0
Kr		40.4	−2.1	8.3	17.2	**0.5**	21.7
Xe		35.3	−3.3	6.4	14.6	**−0.7**	18.6
Rn		30.0	−4.1	4.8	12.1	**−1.4**	15.5
Uuo		27.0	−4.2	4.0	10.7	**−1.5**	13.7
168 e^-		23.9	−4.2	3.3	9.3	**−1.6**	12.0
218 e^-		21.8	−4.1	2.9	8.5	**−1.6**	10.9
290 e^-		19.8	−4.0	2.5	7.6	**−1.5**	9.9
MARE		39.9	6.6	10.5	18.4	**5.5**	22.6

The OFDFT results for the kinetic energy are summarized in the upper panel of Table I. Best results for light atoms (He, Ne, and Ar) are provided from PGint, while for heavier atoms (Kr to 290 e^-) the PGS is the most accurate. In fact both PGint and PGS have a similar overall performance, with MARE ≈ 4.5%, followed by PG20/9 with MARE ≈ 7.2%. The worst results are found from TFW, which underestimates the KE with about 22% on average. We also remark that PG20/9 and PGint are the only functionals which slightly overestimate the KE, with the exception of He atom.

In the lower panel of Table I, we also report the kinetic energies computed using the accurate KSDFT densities. This is a common practice for the testing and assessment of KE functionals [78]. We can see that TFW strongly overestimates the KE by about 40%, showing that (i) the density plays a crucial role and (ii) TFW is not a stable functional. We recall that TFW is still one of the most used KE approximations in OFDFT applications [147,148] and hydrodynamical models for quantum plasmonics [149]. On the other hand, the most

TABLE II. Density error D_0 of Eq. (25) (upper panel), and ionization density error $D_{IP,0}$ of Eq. (26) (lower panel), for noble gas nonrelativistic atoms ($2 \leqslant Z \leqslant 290$). Best result of each line is shown in bold style. Last line reports the MAE in a.u.

Atom	TFW	PG$\frac{20}{9}$	PGS	PG1	PGint	LKT
			Density error $D_0 \times 10^3$			
He	751	**347**	451	535	363	582
Ne	340	**291**	311	325	297	324
Ar	279	275	263	268	**260**	270
Kr	194	190	184	187	**182**	188
Xe	172	167	161	162	**159**	164
Rn	137	130	126	127	**125**	129
Uuo	117	112	110	111	**108**	112
$168e^-$	99.3	92.9	91.5	92.7	**90.4**	94.0
$218e^-$	86.1	81.5	80.4	81.4	**78.8**	82.2
$290e^-$	77.3	70.7	70.6	72.0	**69.0**	72.9
MAE	225.3	175.7	184.8	196.1	**173.2**	201.8
			Ionization density error $D_{IP,0} \times 10^3$			
He	1021	**530**	677	785	557	835
Ne	851	**479**	667	759	561	764
Ar	324	**170**	288	337	231	309
Kr	220	**181**	257	281	242	245
Xe	**162**	247	194	201	197	172
Rn	225	273	227	**204**	220	211
Uuo	377	381	336	320	**315**	338
$168e^-$	446	420	379	369	**351**	393
$218e^-$	565	514	472	468	**438**	499
$290e^-$	624	557	516	515	**477**	550
MAE	481.5	375.2	401.3	423.9	**359.0**	431.6

accurate functionals are PG20/9 and PGint with MARE $\leqslant$ 7%, both of them slightly underestimating the total KE of heavy atoms.

The best overall performance is found from PGint, that improves significantly over the TFW, but still shows a large variance between the OFDFT self-consistent and KSDFT non-self-consistent results of Table I. This fact suggests that the PGint OFDFT density is quite different from the exact KSDFT one. Same trend is found in Table S1 of Ref. [118] for the alkaline earth atoms.

C. Density and radial ionization density errors

In the upper panel of Table II, we show the density error [15]

$$D_0 = \frac{1}{N} \int d\mathbf{r} \, \left| \rho^{\mathrm{KSDFT}}(\mathbf{r}) - \rho^{\mathrm{OFDFT}}(\mathbf{r}) \right|, \tag{25}$$

for the same set of noble atoms. For light atoms (He and Ne), PG20/9 is the most accurate, being closely followed by PGint. While for the other atoms (Ar to 290 e$^-$), PGint and PGS give the best results. Overall, PGint has the smallest mean absolute error (MAE) of 173.2, and TFW is the worst with MAE=225.3. We also mention that the heavier the atom is, the more accurate OFDFT density is obtained.

In Fig. 7, we show a comparison between the worst (TFW) and best (PG20/9) functionals for Ne atom. Neither

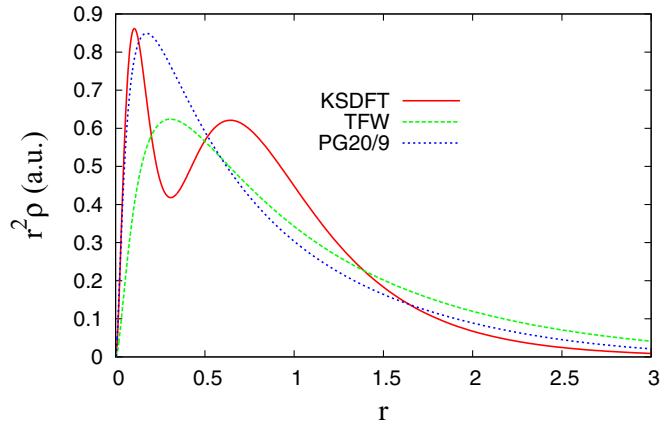

FIG. 7. Comparison of OFDFT TFW and PG20/9 radial densities $[r^2\rho(r)]$ with the KSDFT one, for Ne atom.

one shows the atomic shell structure. However, the PG20/9 density is remarkably accurate near the nucleus, and improves significantly over the TFW one, which is too shallow, giving a too small KE (see Table I).

Next, in the lower panel of Table II, we report the ionization density error

$$D_{IP,0} = \int d\mathbf{r} \, \left| \rho_{IP}^{\mathrm{KSDFT}}(\mathbf{r}) - \rho_{IP}^{\mathrm{OFDFT}}(\mathbf{r}) \right|, \tag{26}$$

where

$$\rho_{IP}(\mathbf{r}) = \rho^{\mathrm{atom}}(\mathbf{r}) - \rho^{\mathrm{ion}}(\mathbf{r}) \tag{27}$$

is the ionization density [$\int d\mathbf{r} \, \rho_{IP}(\mathbf{r}) = 1$]. In this case, the error $D_{IP,0}$ does not decrease for heavy atoms. The best results are again found from PG20/9 (MAE = 375) and PGint (MAE = 359) functionals, which are the most accurate for lighter atoms (He to Kr), and heavy atoms (Uuo to 290 e$^-$), respectively. On the other hand, the worst performances are given by TFW (MAE = 482), LKT (MAE = 432), and PG1 (MAE = 424).

The errors D_0 and $D_{IP,0}$ of Eqs. (25) and Eq. (26), respectively, are biased toward the valence and tail regions. In Table S2 of Ref. [118], we report the errors of $\mathcal{D}_0 = \frac{1}{N} \int_0^\infty dr \, |\rho^{\mathrm{KSDFT}}(r) - \rho^{\mathrm{OFDFT}}(r)|$ (upper panel), and $\mathcal{D}_{IP,0} = \int_0^\infty dr \, |\rho_{IP}^{\mathrm{KSDFT}}(r) - \rho_{IP}^{\mathrm{OFDFT}}(r)|$ (lower panel), which are biased toward the nuclear and inner atomic core regions. In this case, PGS and PGint are the most accurate for $\mathcal{D}_0$, while all functionals perform very similar for $\mathcal{D}_{IP,0}$.

In order to visualize the functional performance for the ionization potential, we report in Fig. 8 a comparison between the KSDFT and PGint OFDFT radial ionization densities $4\pi r^2 \rho_{IP}(\mathbf{r})$, for Ar and Xe atoms. For these atoms, the PGint ionization density is unable to describe the exact behavior in the atomic core, most probably because the OFDFT calculations do not capture the atomic shell oscillations. However, the PGint ionization densities are accurate in the valence and tail regions. This is an important achievement of PGint KE functional, and further tests for nanoparticles and clusters should be done.

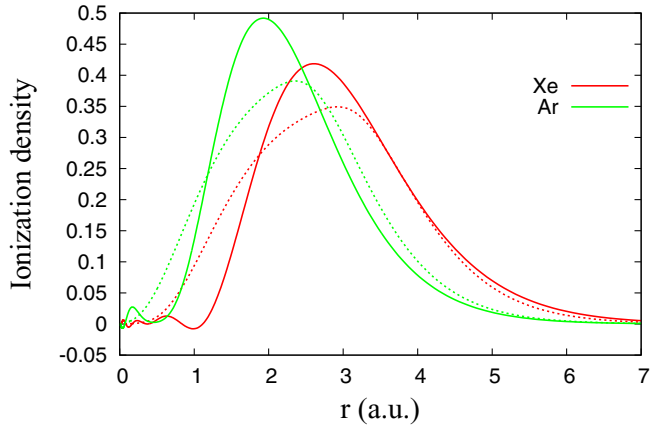

FIG. 8. Radial ionization density $4\pi r^2 \rho_{IP}(\mathbf{r})$ versus the radial distance r for the KSDFT (thick lines) and for OFDFT calculations using the PGint GGA KE functional (dotted lines), for Ar and Xe atoms. The integral under each curve is the number of ionized electrons ($N = 1$).

Finally, in Fig. 9, we show the KSDFT and OFDFT ionization energies of noble atoms. The TFW, LKT, and PG1 results vary very little from He to heavy atoms, and the curves are quite flat. Better shapes are found from PG20/9 and PGint functionals, but the improvement is small. In the semiclassical limit $Z \to \infty$, all OFDFT should presumably be close to the extended Thomas-Fermi (ETF) theory which gives $IP_\infty^{\rm ETF} \approx 0.11$ Ha [146]. However, smooth extrapolations to $Z \to \infty$ predict $IP_\infty^{\rm OFDFT} \approx 0.4$ Ha.

D. Kinetic energy response in atoms

The linear response DFT formalism in atoms has been theoretically investigated [150–153], and the linear response function $\chi(\mathbf{r}, \mathbf{r}')$ is nowadays used in the conceptual DFT as one of the most important reactivity descriptor [154–164]. Because of the use of perturbation theory for degenerate electrons with a given quantum number n, it cannot be found a simple formula as in the case of the uniform electron gas, where the Lindhard function plays the main role [31]. Here we

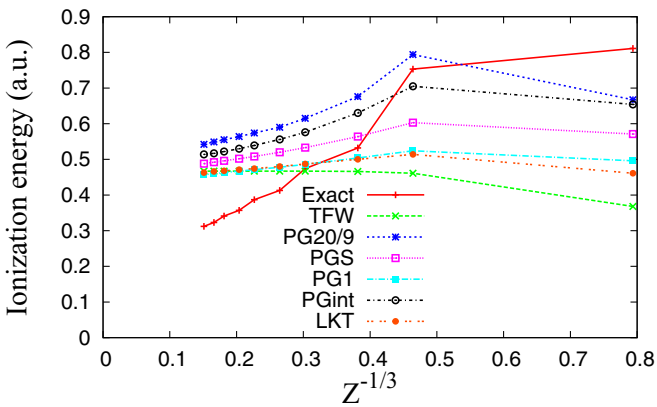

FIG. 9. Ionization energy of noble atoms ($2 \leqslant Z \leqslant 290$) versus $Z^{-1/3}$, computed from KSDFT and OFDFT with several KE GGA functionals, respectively. Here Z is the nuclear charge.

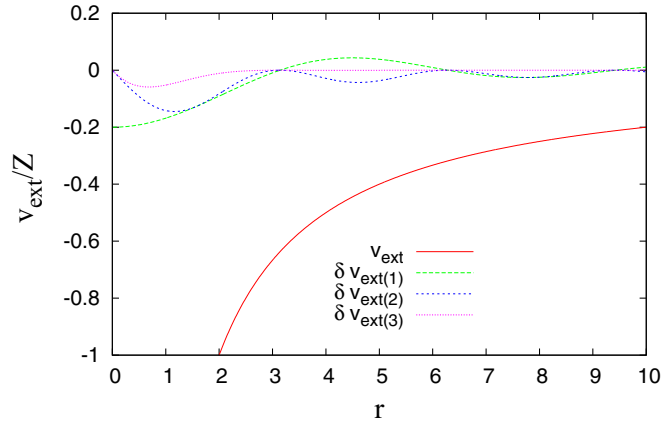

FIG. 10. Comparison of normalized potentials $v_{\rm ext}/Z$, and $\delta v_i^{(M=10)}/Z = (v_i^{(M=10)} - v_{\rm ext})/Z$, with $i = 1$, 2, and 3 [see Eq. (28)].

tested atoms in perturbed external potentials of the following forms:

$$\begin{aligned} v_{\rm ext}(r) &\to v_1^M(r) = v_{\rm ext}(r) + v_{\rm ext}(r)\sin(r)/M, \\ v_{\rm ext}(r) &\to v_2^M(r) = v_{\rm ext}(r) + v_{\rm ext}(r)\sin^2(r)/M, \\ v_{\rm ext}(r) &\to v_3^M(r) = v_{\rm ext}(r) + v_{\rm ext}(r)\sin^2(r)e^{-r}/M, \end{aligned} \tag{28}$$

where $v_{\rm ext}(r) = -Z/r$, and M is a constant. We consider the cases $M = 10$ (a.i. small perturbation where linear response can be accurate), and $M = 3$ (a.i. large perturbation where terms beyond linear response may be important). By construction, $v_i^M(r)$ are very different one to the other: $v_1^M(r)$ has a finite nonzero value at the nucleus, where the density is large and thus will give a significant deviation of the KE. $v_2^M(r)$ and $v_3^M(r)$ vanish at the nucleus, but while $v_2^M(r)$ has a long-range $(1/r)$ decay in the tail of the density, $v_3^M(r)$ is exponentially small. In Fig. 10, we show a comparison of the normalized potentials $v_{\rm ext}/Z$, and $\delta v_i^{(M=10)}/Z = (v_i^{(M=10)} - v_{\rm ext})/Z$, with $i = 1$, 2, and 3.

For all these cases and the tested KE functionals, we calculate the self-consistent KE response

$$\delta T_s = T_s[v_{\rm ext}] - T_s\big[v_i^M\big], \quad i = 1, 2, 3, \quad M = 10 \text{ and } \mathrm{M} = 3. \tag{29}$$

The Ne and Rn results are summarized in Table III. In the case of the perturbed Ne atom, best performances are obtained with PG20/9 (MARE = 22.6%) and PGint KE functionals (MARE = 24.6%), that are almost twice better than TFW (MARE = 44.7%). However, they are not accurate for the localized perturbations of $v_3^{M=3}$ and $v_3^{M=10}$, where the solid-state designed LKT and PG1 functionals are more appropriate. On the other hand, for the perturbed Rn atom, PGint shows best overall results (MARE = 8.1%), but all functionals give good KE atomic responses, with MARE below 10.5%.

Next, we consider the error of the perturbed density $\rho_P(\mathbf{r}) = \rho^{\rm atom}(\mathbf{r}) - \rho^{\rm perturbed\ atom}(\mathbf{r})$

$$D_{P,0} = \int d\mathbf{r}\, \left|\rho_P^{\rm KSDFT}(\mathbf{r}) - \rho_P^{\rm OFDFT}(\mathbf{r})\right|. \tag{30}$$

Note that $\int d\mathbf{r}\ \rho_P(\mathbf{r}) = 0$. This test shows in more detail the OFDFT accuracy for perturbed atoms.

TABLE III. KSDFT KE energy response δT_s (in a.u.), and relative errors in % ([approx-exact]/exact × 100), of δT_s computed self-consistently, within the OFDFT scheme, using several KE approximations, for the perturbed Ne atom (upper panel) and Rn atom (lower panel), subject to external potentials of Eq. (28). Last lines of the panels report the MAREs in %. Best result of each line is shown in bold style.

	KS	TFW	PG$\frac{20}{9}$	PGS	PG1	PGint	LKT
			Perturbed Ne atom				
$v_1^{M=10}$	2.143	31.82	**−0.47**	13.35	20.16	6.07	21.75
$v_1^{M=3}$	5.997	27.81	**0.20**	10.79	16.57	5.00	18.28
$v_2^{M=10}$	−0.983	−96.13	**−25.53**	−58.29	−72.23	−43.03	−74.47
$v_2^{M=3}$	−3.729	−66.40	**−15.02**	−37.33	−48.22	−26.39	−49.69
$v_3^{M=10}$	0.546	15.75	−50.73	−23.44	−11.36	−35.71	**−6.41**
$v_3^{M=3}$	1.561	30.49	−43.56	−16.59	**−1.67**	−31.45	4.10
MARE	–	44.7	**22.6**	26.6	28.4	24.6	29.1
			Perturbed Rn atom				
$v_1^{M=10}$	96.935	−6.35	−8.80	−7.71	−7.24	**−6.19**	−7.21
$v_1^{M=3}$	261.228	**−7.61**	−10.71	−9.60	−9.00	−8.55	−8.84
$v_2^{M=10}$	−93.952	16.28	10.84	12.38	13.74	**8.88**	14.31
$v_2^{M=3}$	−377.832	7.86	3.87	5.14	6.12	**3.16**	6.47
$v_3^{M=10}$	−13.906	−11.43	**−6.72**	−8.38	−9.31	−15.70	−9.56
$v_3^{M=3}$	−50.542	12.24	15.09	13.63	13.15	**6.50**	13.33
MARE	–	10.3	9.3	9.5	9.8	**8.2**	9.9

In Table IV we report the results. We observe the same classification of the functionals as in Table III: PG20/9 and PGint are the best, while TFW is the worst. The total performance of the PG20/9 and PGint KE functionals shows a significant and systematic improvement over the other tested functionals (PGS, PG1, LKT, and TFW), due to the (partial) recovery of the GSE2.

TABLE IV. The perturbed density errors $D_{P,0}$ [see Eq. (30)], for the Ne and Rn atoms subject to the external potentials of Eq. (28). Last lines of the panels report the MAEs. Best result of each line is shown in bold style.

	TFW	PG$\frac{20}{9}$	PGS	PG1	PGint	LKT
		Perturbed Ne atom				
$v_1^{M=10}$	0.83	**0.40**	0.59	0.71	0.47	0.71
$v_1^{M=3}$	1.60	**0.92**	1.21	1.40	1.03	1.41
$v_2^{M=10}$	0.62	**0.24**	0.39	0.51	0.29	0.51
$v_2^{M=3}$	1.31	**0.60**	0.85	1.09	0.69	1.09
$v_3^{M=10}$	0.26	**0.16**	0.21	0.23	0.18	0.23
$v_3^{M=3}$	0.79	**0.47**	0.61	0.70	0.52	0.70
MAE	0.90	**0.47**	0.64	0.77	0.53	0.77
		Perturbed Rn atom				
$v_1^{M=10}$	4.96	4.73	4.68	4.74	**4.44**	4.82
$v_1^{M=3}$	7.39	6.92	6.99	7.14	**6.68**	7.22
$v_2^{M=10}$	4.83	4.79	4.71	4.72	**4.54**	4.77
$v_2^{M=3}$	**7.25**	7.40	7.43	7.43	7.39	7.38
$v_3^{M=10}$	2.33	2.13	2.13	2.20	**2.00**	2.24
$v_3^{M=3}$	5.79	5.32	5.38	5.53	**5.07**	5.61
MAE	5.4	5.2	5.2	5.3	**5.0**	5.3

E. Jellium clusters

The UEG linear response of any GGA functional that recovers GSE2 at small reduced gradient is failing badly in almost all the wave vector space, as shown in Fig. 1. Then, in order to understand the behavior of such KE functionals, for finite jellium systems, we present in Fig. 11 a comparison of several electron densities of a 18 e^- jellium sphere with bulk parameter $r_s = 2.07$. Here we use an accuracy criterion less than 10^{-4} in the absolute value of the maximum deviation between the effective potentials (see Eq. (2) of Ref. [5]) of successive iterations. The PG20/9 and PGint calculations have been performed using a smaller mixing ratio between the effective potentials of two successive iterations and require a large number of iterations.

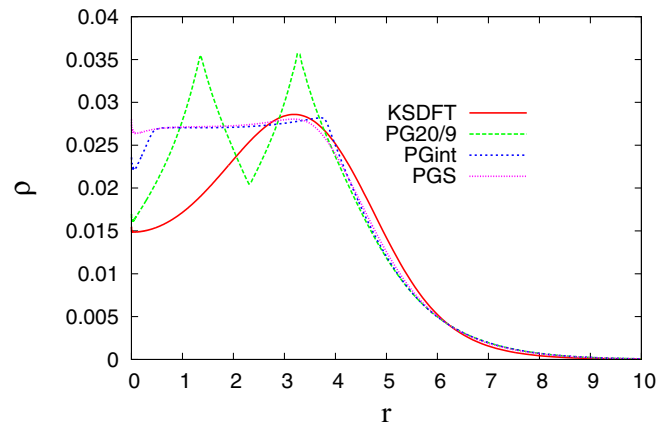

FIG. 11. Electron densities $\rho(r)$ of the jellium sphere with 18 e^- and bulk parameter $r_s = 2.07$, computed from KSDFT and OFDFT with several KE functionals.

The PG20/9 functional, which has the UEG linear response of GSE2, is the most accurate at $r \to 0$ but shows large and spurious Friedel oscillations inside the sphere. This is the right physical behavior expected from GSE2, which, by construction, is overestimating the Friedel oscillations. On the other hand, the PGint, whose UEG linear response is the same as PGS (and GE2), gives a small drop of the density at the center of the cluster but rapidly recovers the PGS behavior.

IV. CONCLUSIONS

We have constructed the nonempirical second-order gradient singularity expansion (GSE2) of the kinetic energy, which can accurately mimic the exact behaviors of both Pauli potential v^θ and KE density τ of atoms, with the exception of the asymptotic and near-the-nucleus regions, where the KE nonlocality cannot be described at the semilocal level. Nevertheless, GSE2 can show the atomic shell structures of v^θ and τ when the KSDFT density is used.

Due to its behavior near the nucleus, the GSE2 alone is not suitable for OFDFT calculations, but it can be used in the development of kinetic energy functionals. In order to study the importance of GSE2 for the semilocal KE functionals, we have constructed the simple PG20/9 GGA KE functional, which is a member of the Pauli-Gaussian-μ family of functionals [15], where $\mu = 20/9$ was chosen to recover the GSE2 in the slowly-varying density regime. The PG20/9 GGA preserves the UEG linear response of GSE2 (see Fig. 1) and has a positive KE Pauli enhancement factor. We have also proposed the PGint GGA KE functional that recovers the regular GE2 in the slowly-varying density regime and for the UEG linear response (see Fig. 1), otherwise being very close to the PG20/9 functional, as shown in Fig. 6.

Using OFDFT calculations, as well as post-processing KSDFT densities, we tested these functionals together with the recently proposed PG1 and PGS [15], LKT [71], and the popular TFW [70], for several properties of noble atoms (from He up to 290 e^- atom): total kinetic energies, ionization energies, density errors, ionization density errors, KE, and electronic density response in atoms due to various changes in the external potential. For all these benchmark tests, the PG20/9 and PGint are between the most accurate, showing a systematic improvement over the other KE functionals. The overall PG20/9 and PGint performance is a strong indication on the usefulness of GSE2 for the KE functional development.

However, still these functionals do not capture the shell-structure oscillations in OFDFT calculations, as shown in Figs. 7 and 8. One of the main reason for this failure can be the modest description of the nuclear region, provided by the GGA level of theory (see also Fig. S3 of Ref. [118], which shows the Pauli KE potentials of Ar and He atoms, computed from OFDFT calculations). We recall that the nuclear region gives a large contribution to the KE. Further investigation of the Laplacian-level meta-GGAs and nonlocal functionals such as u-meta-GGAs [36,77,78] can boost the all-electron OFDFT accuracy for finite systems.

[1] P. Hohenberg and W. Kohn, Phys. Rev. **136**, B864 (1964).
[2] M. Levy, Proc. Natl. Acad. Sci. **76**, 6062 (1979).
[3] W. C. Witt, G. Beatriz, J. M. Dieterich, and E. A. Carter, J. Mater. Res. **33**, 777 (2018).
[4] E. A. Carter, Science **321**, 800 (2008).
[5] M. Levy, J. P. Perdew, and V. Sahni, Phys. Rev. A **30**, 2745 (1984).
[6] G. E. Scuseria and V. N. Staroverov, *Theory and Applications of Computational Chemistry*, edited by C. E. Dykstra, G. Frenking, K. S. Kim, and G. E. Scuseria (Elsevier, Amsterdam, 2005), pp. 669–724.
[7] F. Della Sala, E. Fabiano, and L. A. Constantin, Int. J. Quantum Chem. **116**, 1641 (2016).
[8] M. Levy and J. P. Perdew, Phys. Rev. A **32**, 2010 (1985).
[9] M. Levy, Phys. Rev. A **26**, 1200 (1982).
[10] L. H. Thomas, in *Mathematical Proceedings of the Cambridge Philosophical Society* (Cambridge University Press, Cambridge, 1927), Vol. 23, pp. 542–548.
[11] E. Fermi, Rend. Accad. Naz. Lincei **6**, 32 (1927).
[12] V. V. Karasiev, D. Chakraborty, and S. B. Trickey, *Many-Electron Approaches in Physics, Chemistry and Mathematics* (Springer, Cham, 2014), pp. 113–134.
[13] V. V. Karasiev and S. B. Trickey, Adv. Quantum Chem. **71**, 221 (2015).
[14] L. A. Constantin, E. Fabiano, and F. Della Sala, Phys. Rev. B **97**, 205137 (2018).
[15] L. A. Constantin, E. Fabiano, and F. Della Sala, J. Phys. Chem. Lett. **9**, 4385 (2018).
[16] T. T. Chau, J. H. Hue, M.-I. Trappe, and B.-G. Englert, New J. Phys. **20**, 073003 (2018).
[17] L. Hung and E. A. Carter, Chem. Phys. Lett. **475**, 163 (2009).
[18] F. Lambert, J. Clérouin, and S. Mazevet, Europhys. Lett. **75**, 681 (2006).
[19] M. Chen, L. Hung, C. Huang, J. Xia, and E. A. Carter, Mol. Phys. **111**, 3448 (2013).
[20] V. Gavini, K. Bhattacharya, and M. Ortiz, J. Mech. Phys. Sol. **55**, 697 (2007).
[21] B. Radhakrishnan and V. Gavini, Phys. Rev. B **82**, 094117 (2010).
[22] V. Gavini, Phys. Rev. Lett. **101**, 205503 (2008).
[23] B. Radhakrishnan and V. Gavini, Philos. Mag. **96**, 2468 (2016).
[24] K. J. Caspersen and E. A. Carter, Proc. Nat. Acad. Sc. **102**, 6738 (2005).
[25] H. Xiang, M. Zhang, X. Zhang, and G. Lu, J. Phys. Chem. C **120**, 14330 (2016).
[26] B. G. del Rio, M. Chen, L. E. González, and E. A. Carter, J. Chem. Phys. **149**, 094504 (2018).
[27] G. Ho, M. T. Ong, K. J. Caspersen, and E. A. Carter, Phys. Chem. Chem. Phys. **9**, 4951 (2007).
[28] I. Shin and E. A. Carter, Acta Mater. **64**, 198 (2014).
[29] W. Mi and M. Pavanello, arXiv:1812.08952.

[30] P. García-González, J. E. Alvarellos, and E. Chacón, Phys. Rev. A **54**, 1897 (1996).

[31] Y. A. Wang and E. A. Carter, *Theoretical Methods in Condensed Phase Chemistry* (Springer, New York, 2002), pp. 117–184.

[32] I. A. Howard, N. H. March, and V. E. Van Doren, Phys. Rev. A **63**, 062501 (2001).

[33] N. March and R. Santamaria, Int. J. Quantum Chem. **39**, 585 (1991).

[34] F. Della Sala, E. Fabiano, and L. A. Constantin, Phys. Rev. B **91**, 035126 (2015).

[35] J. C. Snyder, M. Rupp, K. Hansen, K.-R. Müller, and K. Burke, Phys. Rev. Lett. **108**, 253002 (2012).

[36] L. A. Constantin, E. Fabiano, and F. Della Sala, Computation **4**, 19 (2016).

[37] R. O. Esquivel, J. Chen, M. J. Stott, R. P. Sagar, and V. H. Smith Jr, Phys. Rev. A **47**, 936 (1993).

[38] J. Sun, B. Xiao, Y. Fang, R. Haunschild, P. Hao, A. Ruzsinszky, G. I. Csonka, G. E. Scuseria, and J. P. Perdew, Phys. Rev. Lett. **111**, 106401 (2013).

[39] Z. Qian, Phys. Rev. B **75**, 193104 (2007).

[40] L. A. Constantin, E. Fabiano, J. M. Pitarke, and F. Della Sala, Phys. Rev. B **93**, 115127 (2016).

[41] M. Ernzerhof, K. Burke, and J. P. Perdew, J. Chem. Phys. **105**, 2798 (1996).

[42] A. D. Becke and K. E. Edgecombe, J. Chem. Phys. **92**, 5397 (1990).

[43] E. Fabiano, L. Constantin, and F. Della Sala, J. Chem. Theory Comput. **10**, 3151 (2014).

[44] Y. Han and D.-J. Liu, Phys. Rev. B **80**, 155404 (2009).

[45] C. F. von Weizsäcker, Z. Phys. **96**, 431 (1935).

[46] K. Finzel, Int. J. Quantum Chem. **115**, 1629 (2015).

[47] K. Finzel, Int. J. Quantum Chem. **116**, 1261 (2016).

[48] K. Finzel, J. Davidsson, and I. A. Abrikosov, Int. J. Quantum Chem. **116**, 1337 (2016).

[49] K. Finzel, J. Chem. Phys. **144**, 034108 (2016).

[50] K. Finzel, Theor. Chem. Acc. **135**, 87 (2016).

[51] K. Finzel, Theor. Chem. Acc. **134**, 106 (2015).

[52] K. Finzel and P. W. Ayers, Int. J. Quantum Chem. **117**, e25364 (2017).

[53] K. Finzel, Theor. Chem. Acc. **135**, 148 (2016).

[54] K. Finzel, Int. J. Quantum Chem. **117**, e25329 (2017).

[55] D. Kirzhnitz, Sov. Phys. JETP **5**, 64 (1957).

[56] H. Ou-Yang and M. Levy, Int. J. Quantum Chem. **40**, 379 (1991).

[57] J. P. Perdew, Phys. Lett. A **165**, 79 (1992).

[58] M. Ernzerhof, J. Mol. Struct.: THEOCHEM **501**, 59 (2000).

[59] L. A. Constantin and A. Ruzsinszky, Phys. Rev. B **79**, 115117 (2009).

[60] L. Vitos, B. Johansson, J. Kollar, and H. L. Skriver, Phys. Rev. A **61**, 052511 (2000).

[61] A. Lindmaa, A. E. Mattsson, and R. Armiento, Phys. Rev. B **90**, 075139 (2014).

[62] L. A. Constantin, E. Fabiano, S. Śmiga, and F. Della Sala, Phys. Rev. B **95**, 115153 (2017).

[63] A. Borgoo and D. J. Tozer, J. Chem. Theory Comput. **9**, 2250 (2013).

[64] A. J. Thakkar, Phys. Rev. A **46**, 6920 (1992).

[65] A. Lembarki and H. Chermette, Phys. Rev. A **50**, 5328 (1994).

[66] J. Seino, R. Kageyama, M. Fujinami, Y. Ikabata, and H. Nakai, J. Chem. Phys. **148**, 241705 (2018).

[67] V. V. Karasiev, T. Sjostrom, and S. B. Trickey, Comput. Phys. Commun. **185**, 3240 (2014).

[68] V. V. Karasiev, S. B. Trickey, and F. E. Harris, J. Comput.-Aided Mater. Des. **13**, 111 (2006).

[69] V. V. Karasiev, D. Chakraborty, O. A. Shukruto, and S. B. Trickey, Phys. Rev. B **88**, 161108(R) (2013).

[70] J. Xia and E. A. Carter, Phys. Rev. B **91**, 045124 (2015).

[71] K. Luo, V. V. Karasiev, and S. B. Trickey, Phys. Rev. B **98**, 041111(R) (2018).

[72] M. Brack, B. K. Jennings, and Y. H. Chu, Phys. Lett. B **65**, 1 (1976).

[73] C. H. Hodges, Can. J. Phys. **51**, 1428 (1973).

[74] A. C. Cancio, D. Stewart, and A. Kuna, J. Chem. Phys. **144**, 084107 (2016).

[75] A. C. Cancio and J. J. Redd, Mol. Phys. **115**, 618 (2017).

[76] P. Golub and S. Manzhos, Phys. Chem. Chem. Phys. **21**, 378 (2019).

[77] L. A. Constantin, E. Fabiano, and F. Della Sala, J. Chem. Phys. **145**, 084110 (2016).

[78] L. A. Constantin, E. Fabiano, and F. Della Sala, J. Chem. Theory Comput. **13**, 4228 (2017).

[79] C. Huang and E. A. Carter, Phys. Rev. B **81**, 045206 (2010).

[80] Y. A. Wang, N. Govind, and E. A. Carter, Phys. Rev. B **58**, 13465 (1998).

[81] I. Shin and E. A. Carter, J. Chem. Phys. **140**, 18A531 (2014).

[82] G. S. Ho, V. L. Lignères, and E. A. Carter, Phys. Rev. B **78**, 045105 (2008).

[83] J. A. Alonso and L. A. Girifalco, Phys. Rev. B **17**, 3735 (1978).

[84] P. García-González, J. E. Alvarellos, and E. Chacón, Phys. Rev. B **53**, 9509 (1996).

[85] E. Chacón, J. E. Alvarellos, and P. Tarazona, Phys. Rev. B **32**, 7868 (1985).

[86] P. García-González, J. E. Alvarellos, and E. Chacón, Phys. Rev. B **57**, 4857 (1998).

[87] D. Garcia-Aldea and J. E. Alvarellos, Phys. Rev. A **77**, 022502 (2008).

[88] W. Mi, A. Genova, and M. Pavanello, J. Chem. Phys. **148**, 184107 (2018).

[89] E. V. Ludeña, E. X. Salazar, M. H. Cornejo, D. E. Arroyo, and V. V. Karasiev, Int. J. Quantum Chem. **118**, e25601 (2018).

[90] E. X. Salazar, P. F. Guarderas, E. V. Ludena, M. H. Cornejo, and V. V. Karasiev, Int. J. Quantum Chem. **116**, 1313 (2016).

[91] K. Mills, M. Spanner, and I. Tamblyn, Phys. Rev. A **96**, 042113 (2017).

[92] F. Brockherde, L. Vogt, L. Li, M. E. Tuckerman, K. Burke, and K.-R. Müller, Nat. Commun. **8**, 872 (2017).

[93] L. Li, T. E. Baker, S. R. White, and K. Burke, Phys. Rev. B **94**, 245129 (2016).

[94] J. C. Snyder, M. Rupp, K. Hansen, L. Blooston, K.-R. Müller, and K. Burke, J. Chem. Phys. **139**, 224104 (2013).

[95] T. L. Fletcher, S. M. Kandathil, and P. L. Popelier, Theor. Chem. Acc. **133**, 1499 (2014).

[96] V. Botu, R. Batra, J. Chapman, and R. Ramprasad, J. Phys. Chem. C **121**, 511 (2016).

[97] L. Li, J. C. Snyder, I. M. Pelaschier, J. Huang, U.-N. Niranjan, P. Duncan, M. Rupp, K.-R. Müller, and K. Burke, Int. J. Quantum Chem. **116**, 819 (2016).

[98] D. Pettifor and M. Ward, Solid State Commun. **49**, 291 (1984).

[99] P. Sprunger, L. Petersen, E. Plummer, E. Lægsgaard, and F. Besenbacher, Science **275**, 1764 (1997).

[100] G. Gruner, *Density Waves in Solids* (CRC Press, Boca Raton, 2018).

[101] J.-D. Chai and J. D. Weeks, Phys. Rev. B **75**, 205122 (2007).

[102] J.-D. Chai and J. D. Weeks, J. Phys. Chem. B **108**, 6870 (2004).

[103] M. P. Das and F. Green, J. Phys.: Conf. Ser. **726**, 012001 (2016).

[104] A. Landa, P. Soederlind, I. Naumov, J. Klepeis, and L. Vitos, Computation **6**, 29 (2018).

[105] Z. H. Levine and S. G. Louie, Phys. Rev. B **25**, 6310 (1982).

[106] J. Callaway, Phys. Rev. **116**, 1368 (1959).

[107] D. R. Penn, Phys. Rev. **128**, 2093 (1962).

[108] G. Srinivasan, Phys. Rev. **178**, 1244 (1969).

[109] A. Tsolakidis, E. L. Shirley, and R. M. Martin, Phys. Rev. B **69**, 035104 (2004).

[110] J. Rey and A. Savin, Int. J. Quantum Chem. **69**, 581 (1998).

[111] J. B. Krieger, J. Chen, G. J. Iafrate, and A. Savin, in *Electron Correlations and Materials Properties*, edited by A. Gonis, N. Kioussis, and M. Ciftan (Kluwer Academic, New York, 1999), p. 463.

[112] J. B. Krieger, J. Chen, and S. Kurth, in *Density Functional Theory and its Application to Materials*, edited by V. Van Doren, C. Van Alsenoy and P. Geerlings, AIP Conf. Proc. No. 577 (AIP, New York, 2001), p. 48.

[113] J. Toulouse, A. Savin, and C. Adamo, J. Chem. Phys. **117**, 10465 (2002).

[114] J. Toulouse and C. Adamo, Chem. Phys. Lett. **362**, 72 (2002).

[115] E. Fabiano, P. E. Trevisanutto, A. Terentjevs, and L. A. Constantin, J. Chem. Theory. Comput. **10**, 2016 (2014).

[116] A. V. Terentjev, L. A. Constantin, and J. M. Pitarke, Phys. Rev. B **98**, 085123 (2018).

[117] J. Tao, J. P. Perdew, L. M. Almeida, C. Fiolhais, and S. Kümmel, Phys. Rev. B **77**, 245107 (2008).

[118] See Supplemental Material at http://link.aps.org/supplemental/10.1103/PhysRevB.99.155137 for derivation of Eq. (12); Err(β) of Eq. (22) for various atoms; GSE2 Pauli potential for Mg and Zn atoms; OFDFT calculations for alkaline earth atoms; other definition of density error; and Pauli potential from OFDFT calculations.

[119] G. S. Ho, V. L. Lignères, and E. A. Carter, Comput. Phys. Commun. **179**, 839 (2008).

[120] S. Śmiga, E. Fabiano, S. Laricchia, L. A. Constantin, and F. Della Sala, J. Chem. Phys. **142**, 154121 (2015).

[121] S. Śmiga, E. Fabiano, L. A. Constantin, and F. Della Sala, J. Chem. Phys. **146**, 064105 (2017).

[122] D. Mejia-Rodriguez and S. B. Trickey, Phys. Rev. A **96**, 052512 (2017).

[123] F. Tran, P. Kovács, L. Kalantari, G. K. Madsen, and P. Blaha, J. Chem. Phys. **149**, 144105 (2018).

[124] D. Garcia-Aldea and J. Alvarellos, J. Chem. Phys. **129**, 074103 (2008).

[125] E. Engel and S. H. Vosko, Phys. Rev. A **47**, 2800 (1993).

[126] E. Engel, *A Primer in Density Functional Theory* (Springer, New York, 2003), pp. 56–122.

[127] Á. Nagy, Int. J. Quantum Chem. **106**, 1043 (2006).

[128] M. Levy and H. Ou-Yang, Phys. Rev. A **38**, 625 (1988).

[129] E. Fabiano, L. A. Constantin, and F. Della Sala, Int. J. Quantum Chem. **113**, 673 (2013).

[130] E. Fabiano, L. A. Constantin, and F. D. Sala, J. Chem. Phys. **134**, 194112 (2011).

[131] L. A. Constantin, L. Chiodo, E. Fabiano, I. Bodrenko, and F. Della Sala, Phys. Rev. B **84**, 045126 (2011).

[132] L. A. E. Leal, A. Karpenko, M. A. Caro, and O. Lopez-Acevedo, Phys. Chem. Chem. Phys. **17**, 31463 (2015).

[133] G. K.-L. Chan, A. J. Cohen, and N. C. Handy, J. Chem. Phys. **114**, 631 (2001).

[134] P. Elliott, D. Lee, A. Cangi, and K. Burke, Phys. Rev. Lett. **100**, 256406 (2008).

[135] E. Fabiano and L. A. Constantin, Phys. Rev. A **87**, 012511 (2013).

[136] J. Lehtomäki and O. Lopez-Acevedo, J. Chem. Phys. **147**, 234102 (2017).

[137] A. Cancio, G. P. Chen, B. T. Krull, and K. Burke, J. Chem. Phys. **149**, 084116 (2018).

[138] K. Burke, A. Cancio, T. Gould, and S. Pittalis, J. Chem. Phys. **145**, 054112 (2016).

[139] P. Elliott and K. Burke, Can. J. Chem. **87**, 1485 (2009).

[140] J. Lehtomäki, I. Makkonen, M. A. Caro, A. Harju, and O. Lopez-Acevedo, J. Chem. Phys. **141**, 234102 (2014).

[141] A. C. Cancio and C. Y. Fong, Phys. Rev. A **85**, 042515 (2012).

[142] A. C. Cancio, C. E. Wagner, and S. A. Wood, Int. J. Quantum Chem. **112**, 3796 (2012).

[143] A. D. Becke, Phys. Rev. A **38**, 3098 (1988).

[144] F. Tran and T. A. Wesołowski, Int. J. Quantum Chem. **89**, 441 (2002).

[145] A. M. Navarrete-López, J. Garza, and R. Vargas, J. Chem. Phys. **128**, 104110 (2008).

[146] L. A. Constantin, J. C. Snyder, J. P. Perdew, and K. Burke, J. Chem. Phys. **133**, 241103 (2010).

[147] P. Motamarri, M. Iyer, J. Knap, and V. Gavini, J. Comput. Phys. **231**, 6596 (2012).

[148] B. G. Radhakrishnan and V. Gavini, *Recent Progress in Orbital-Free Density Functional Theory* (World Scientific, Singapore, 2013), pp. 147–163.

[149] C. Ciracì and F. Della Sala, Phys. Rev. B **93**, 205405 (2016).

[150] M. J. Stott and E. Zaremba, Phys. Rev. A **21**, 12 (1980).

[151] P. Senet, J. Chem. Phys. **107**, 2516 (1997).

[152] M. H. Cohen, M. V. Ganduglia-Pirovano, and J. Kudrnovskỳ, J. Chem. Phys. **103**, 3543 (1995).

[153] S. Liu, T. Li, and P. W. Ayers, J. Chem. Phys. **131**, 114106 (2009).

[154] P. Geerlings, S. Fias, Z. Boisdenghien, and F. De Proft, Chem. Soc. Rev. **43**, 4989 (2014).

[155] A. Savin, F. Colonna, and M. Allavena, J. Chem. Phys. **115**, 6827 (2001).

[156] Z. Boisdenghien, C. Van Alsenoy, F. De Proft, and P. Geerlings, J. Chem. Theory Comput. **9**, 1007 (2013).

[157] Z. Boisdenghien, S. Fias, C. Van Alsenoy, F. De Proft, and P. Geerlings, Phys. Chem. Chem. Phys. **16**, 14614 (2014).

[158] J. G Angyan, Current Organic Chemistry **15**, 3609 (2011).
[159] S. Fias, Z. Boisdenghien, F. De Proft, and P. Geerlings, J. Chem. Phys. **141**, 184107 (2014).
[160] F. De Proft and P. Geerlings, Chem. Rev. **101**, 1451 (2001).
[161] G. Roos, S. Loverix, F. De Proft, L. Wyns, and P. Geerlings, J. Phys. Chem. A **107**, 6828 (2003).
[162] P. A. Johnson, L. J. Bartolotti, P. W. Ayers, T. Fievez, and P. Geerlings, *Modern Charge-Density Analysis* (Springer, Dordrecht, 2011), pp. 715–764.
[163] P. Geerlings and F. De Proft, Phys. Chem. Chem. Phys. **10**, 3028 (2008).
[164] P. Geerlings, P. W. Ayers, A. Toro-Labbé, P. K. Chattaraj, and F. De Proft, Acc. Chem. Res. **45**, 683 (2012).